

Universal dynamics of order parameter fluctuations in pump-probe experiments

Pavel E. Dolgirev,^{1,*} Marios H. Michael,¹ Alfred Zong,² Nuh Gedik,² and Eugene Demler¹

¹*Department of Physics, Harvard University, Cambridge, Massachusetts 02138, USA.*

²*Massachusetts Institute of Technology, Department of Physics, Cambridge, Massachusetts 02139, USA.*

(Dated: May 5, 2022)

Upon excitation by a laser pulse, broken-symmetry phases of a wide variety of solids demonstrate similar order parameter dynamics characterized by a dramatic slowing down of relaxation for stronger pump fluences. Motivated by this recurrent phenomenology, we develop a simple non-perturbative effective model of dynamics of collective bosonic excitations in pump-probe experiments. We find that as the system recovers after photoexcitation, it shows universal prethermalized dynamics manifesting a power-law, as opposed to exponential, relaxation, explaining the slowing down of the recovery process. For strong quenches, long-wavelength over-populated transverse modes dominate the long-time dynamics; their distribution function exhibits universal scaling in time and space, whose universal exponents can be computed analytically. Our model offers a unifying description of order parameter fluctuations in a regime far from equilibrium, and our predictions can be tested with available time-resolved techniques.

In the theory of equilibrium phase transitions, the concept of universality plays a central role because it allows describing a plethora of experimentally studied thermal phase transitions with just a few universality classes [1]. For systems far from equilibrium, the notion of universality is relatively unexplored and has recently emerged as an active field [2–9], partially motivated by recent progress in ultracold-atom [10–13] and ultrafast pump-probe experiments [14]. In a non-equilibrium context, one of the dramatic manifestations of the universality is the emergence of the self-similar evolution of correlation functions [15]. In particular, after a strong perturbation, the transient equal-time two-point correlation function $D(|\mathbf{x} - \mathbf{y}|, t)$ might depend only on a single evolving length scale $\xi(t)$ and two universal functions:

$$D(|\mathbf{x} - \mathbf{y}|, t) = g(t)f(|\mathbf{x} - \mathbf{y}|/\xi(t)). \quad (1)$$

Functional forms of $f(x)$ and $g(t)$ depend neither on microscopic parameters nor on initial conditions. Typical equations of motion, often a complex system of partial integro-differential equations, represent an interplay between many degrees of freedom such as quasiparticles, order parameter (OP), phonons and/or magnons. If these equations allow for the above self-similar form, the analysis might reduce to just a few differential equations, which is particularly appealing since it eases the interpretation of the involved evolution. From a physical standpoint, the self-similarity suggests that there exists a stabilization-like mechanism responsible for this form.

Several recurrent observations in experiments also hint at the existence of universality in the out-of-equilibrium context. Aided by recent advances in pump-probe techniques, light-induced phase transitions have been investigated in a wide variety of materials, including charge-density-wave (CDW) compounds [14, 16–25], excitonic insulators [26, 27], magnetically-ordered systems [28, 29], and systems that exhibit several intertwined orders [30, 31]. Upon photoexcitation, some general phenomenol-

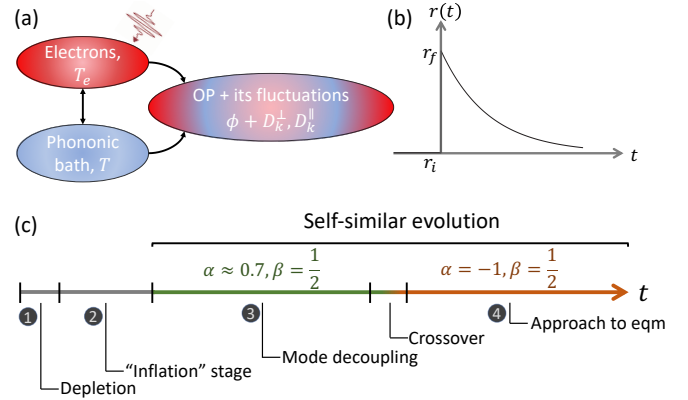


FIG. 1. (Color online) (a) Schematics of a non-equilibrium state: electrons (red) and the phononic bath (blue) are thermal with temperatures $T_e(t)$ and T , respectively; the OP subsystem (mixed colors) is not assumed to be thermal. (b) Time evolution of the Landau coefficient $r(t)$, cf. Eq. (16). It mimics a photoexcitation event in (a). (c) Schematics of dynamical stages experienced by the system after a quench. During stages 3 and 4, the system exhibits self-similarity. Green and orange color codes indicate that the scaling exponents α and β , cf. Eq. (3), are different in these two stages.

ogy is observed: (i) The recovery of a photo-suppressed OP takes longer at stronger pump pulse fluence; (ii) The amplitude of the OP restores faster than the phase, exhibiting a separation of timescales; (iii) Related to (ii), peaks in diffraction experiments remain broadened compared to equilibrium shape long after photoexcitation, showing prolonged suppression of long-range phase coherence. These observations motivate us to search for a unified theoretical description.

A common approach to describing many-body dynamics in pump-probe experiments in states with broken symmetry is based on the so-called three-temperature model (3TM) [32–35], or more generally the N -temperature model (NTM) [36]. In this framework, a

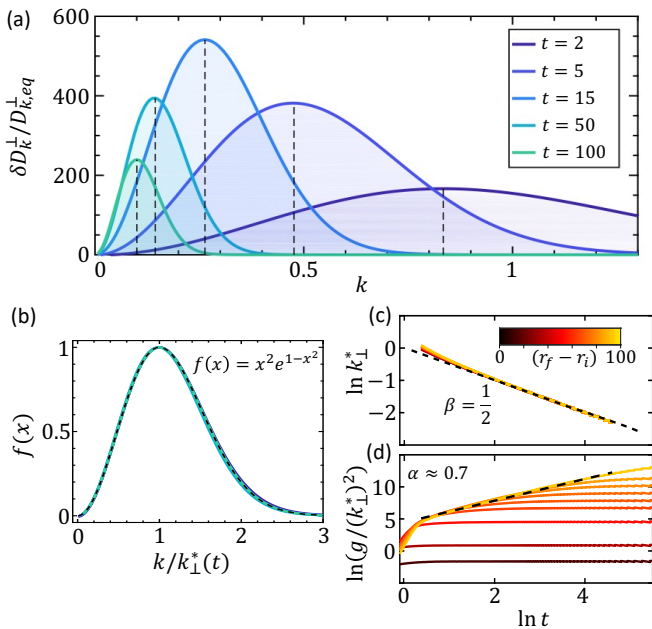


FIG. 2. (Color online) Long-time self-similarity. (a) Time dependence of the change in transverse momentum distribution $\delta D_{\mathbf{k}}^{\perp}$ normalized by the equilibrium value in Eq. (13). Quench strength is set to be $(r_f - r_i) = 80$. Dashed vertical lines track the position of the peak, $k_{\perp}^*(t)$; $g(t)$ corresponds to the peak height. (b) Rescaled curves collapse into $f(x)$, cf. Eq. (2). (c) Evolution of $k_{\perp}^*(t) \sim t^{-\frac{1}{2}}$ at different quench strengths. Note that $k_{\perp}^*(t)$ does not depend on quench. (d) The same for the scaling function $g(t)$. From this figure we extract $\alpha \approx 0.7$, cf. Eq. (3), in the third dynamical stage and $\alpha = -1$ in the final stage.

non-equilibrium state is characterized by assigning different temperatures to different subsystems, such as electrons, phonons, and OP degrees of freedom [37]. Upon photoexcitation, most incoming light is absorbed by electrons, instantaneously increasing the electronic temperature, T_e . The introduction of $T_e(t)$ is justified provided we are only interested in phononic timescales that sufficiently exceed the fast electron-electron scattering time. Subsequent dynamics corresponds to heat exchange between hot electrons and the other two subsystems. In this process, it is often assumed that the lattice heating is negligible because the lattice heat capacity at room temperature is several orders in magnitude larger than that of electrons. Even though the 3TM suggests an intuitive picture about the interplay among different subsystems, it often lacks theoretical justification. In particular, low-energy low-momenta Goldstone modes can be easily excited in the symmetry-broken phase. Hence, one key assumption in the 3TM that the OP subsystem remains thermal is a crude over-simplification.

In this Letter, we go beyond the 3TM and formulate a general theory of out-of-equilibrium OP correlations to account for potentially non-thermal states of the OP subsystem – see Fig. 1a. Our theory focuses on non-linear

dynamics of collective bosonic excitations. This should be contrasted to earlier work on the relaxation of quasiparticles in superconductors, in which recombination dynamics can lead to faster relaxation rates for higher quasiparticle densities [38–40] (see, however, Ref. [41]). Within our effective bosonic model, we find that upon photoexcitation, the system passes through four dynamical stages outlined in Fig. 1c. For a strong quench, not only is the OP subsystem far from being thermal but overpopulated slow Goldstone modes fully dominate the intrinsic evolution at long times. Even more strikingly, in the last two dynamical stages in Fig. 1c, the distribution function of these modes exhibits self-similar evolution as in Eq. (1). With these findings, we can explain all of the mentioned experimental observations.

More specifically, our discovery of self-similarity can be summarized in the following equations. The distribution function of the Goldstone modes follow

$$\delta D_{\mathbf{k}}^{\perp}(t) \simeq \frac{g(t)}{k^2} f(k/k_{\perp}^*(t)), \quad (2)$$

where $\delta D_{\mathbf{k}}^{\perp}(t) \equiv (D_{\mathbf{k}}^{\perp}(t) - D_{\mathbf{k},eq}^{\perp})$ and $D_{\mathbf{k},eq}^{\perp}$ is the pre-pulse equilibrium distribution given by Eq. (13). The form in Eq. (2) is similar to the one in Eq. (1), though written in momentum space; $\xi_{\perp}(t) \equiv (k_{\perp}^*(t))^{-1}$ represents the emergent time-dependent length scale. We also identify the scaling relations

$$g(t) \sim t^{\alpha}, \quad k_{\perp}^* \sim t^{-\beta}. \quad (3)$$

Both power-law exponents α, β and the function $f(x)$ are universal. We find that $\beta = \frac{1}{2}$, while $\alpha \approx 0.7$ at early times and $\alpha = -1$ in the final relaxation stage. The scaling functions $f(x)$, $k_{\perp}^*(t)$, and $g(t)$ are shown in Fig. 2.

We first explore the implications of the self-similarity (2) on the experimental phenomenology. Prior to the arrival of the pump pulse, the system possesses long-range coherence manifested in the macroscopic homogeneous OP ϕ and divergent transverse correlation length $\xi_{\perp} = \infty$. The laser pulse depletes this coherence. The scaling (2) suggests that as the system evolves towards equilibrium, it develops a finite correlation length $\xi_{\perp}(t)$ that slowly grows in a diffusive manner $\xi_{\perp}(t) \sim \sqrt{t}$ [42], consistent with recent experiments [22, 23]. This physical picture explains the broadening of diffraction peaks observed long after the arrival of the pulse. The slowing-down of the OP recovery can also be deduced from Eq. (2). The system enters the final dynamical stage with $g(t) \simeq A_Q t^{-1}$, where A_Q is a constant of proportionality that monotonically increases with the quench strength. By contrast, as shown in Fig. 2c, $k_{\perp}^*(t)$ does not depend on the quench. Therefore, the cumulative effect, expressed in the change of the population of transverse modes $\delta n_{\text{tot}}^{\perp}$, behaves as

$$\delta n_{\text{tot}}^{\perp} \equiv \int \frac{d^3 \mathbf{k}}{(2\pi)^3} \delta D_{\mathbf{k}}^{\perp}(t) \sim A_Q t^{-3/2}, \quad (4)$$

i.e. as a *power-law*. Since the transverse modes dominate the long-time dynamics, from Eq. (4) it follows that characteristic recovery time $\tau_{\text{rec}} \sim A_Q^{2/3}$ is a monotonically increasing function of the quench strength – see also Fig. 3b.

We now explicitly formulate our model and derive the above results. We describe spontaneous symmetry breaking (SSB) in the framework of the time-dependent Landau-Ginzburg formalism (model-A [43, 44]):

$$\frac{d\phi_\alpha(\mathbf{x}, t)}{dt} = -\Gamma \frac{\delta \mathcal{F}}{\delta \phi_\alpha(\mathbf{x}, t)} + \eta_\alpha(\mathbf{x}, t). \quad (5)$$

Here ϕ_α is an N -component vector of real fields representing the OP. The free energy functional reads

$$\mathcal{F}[\phi] = \int d^3\mathbf{x} \left[\frac{r}{2} \phi_\alpha^2 + \frac{K}{2} (\nabla \phi_\alpha)^2 + u(\phi_\alpha^2)^2 \right], \quad (6)$$

and the second term in Eq. (5) represents the noise originating from the phononic bath (with temperature T):

$$\langle \eta_\alpha(\mathbf{x}, t) \eta_\beta(\mathbf{x}', t') \rangle = 2T\Gamma \delta_{\alpha,\beta} \delta(\mathbf{x} - \mathbf{x}') \delta(t - t'). \quad (7)$$

Here r , K , u , and Γ are the model parameters. For homogeneous quenches, without loss of generality, we assume that SSB occurs along the first direction: $\phi(t) = \langle \phi_1(\mathbf{x}, t) \rangle$. Associated with the OP are longitudinal $D_{\mathbf{k}}^{\parallel}(t) \equiv \langle \phi_1(\mathbf{k}; t) \phi_1(-\mathbf{k}; t) \rangle_c$ and transverse $D_{\mathbf{k}}^{\perp}(t) \equiv \langle \phi_{\alpha \neq 1}(\mathbf{k}; t) \phi_{\alpha}(-\mathbf{k}; t) \rangle_c$ correlation functions. In the language of the CDW theory, these correlators represent momentum distribution functions of amplitudons (Higgs modes) and phasons (Goldstone modes), respectively. The model-A formalism (5)–(7) can be conveniently rewritten in terms of the Fokker-Planck equation:

$$\partial_t \mathcal{P} = T\Gamma \sum_{\mathbf{k}, \alpha} \frac{\delta}{\delta \phi_{\alpha, \mathbf{k}}} \left[\frac{\mathcal{P}}{T} \frac{\delta \mathcal{F}}{\delta \phi_{\alpha, -\mathbf{k}}} + \frac{\delta \mathcal{P}}{\delta \phi_{\alpha, -\mathbf{k}}} \right], \quad (8)$$

where $\mathcal{P}([\phi], t)$ is the probability distribution functional of space-dependent field configurations $\phi_\alpha(\mathbf{x})$. To the leading order in $1/N$, $\mathcal{P}([\phi], t)$ is Gaussian, implying that the OP $\phi(t)$ and the correlators $D_{\mathbf{k}}^{\parallel}(t)$, $D_{\mathbf{k}}^{\perp}(t)$ form a closed set of dynamical variables. The self-consistent equations of motion read (see Ref. [45] for the details)

$$\frac{d\phi(t)}{dt} = -\Gamma r_{\text{eff}} \phi, \quad (9)$$

$$\frac{dD_{\mathbf{k}}^{\perp}(t)}{dt} = 2T\Gamma - 2\Gamma(K\mathbf{k}^2 + r_{\text{eff}})D_{\mathbf{k}}^{\perp}, \quad (10)$$

$$\frac{dD_{\mathbf{k}}^{\parallel}(t)}{dt} = 2T\Gamma - 2\Gamma(K\mathbf{k}^2 + r_{\text{eff}} + 8u\phi^2)D_{\mathbf{k}}^{\parallel}. \quad (11)$$

Here the self-consistent “mass”-term is defined as

$$r_{\text{eff}}(t) = r(t) + 4u \left(\phi^2 + n_{\text{tot}}^{\parallel} + (N-1)n_{\text{tot}}^{\perp} \right), \quad (12)$$

where $n_{\text{tot}}^{\perp(\parallel)} \equiv \int^{\Lambda} \frac{d^3\mathbf{q}}{(2\pi)^3} D_{\mathbf{q}}^{\perp(\parallel)}$. Note that quantities such as energy or total number of excitations are not conserved. The presence of the bath, cf. Eq. (7), will also

always result in the thermalization of the system. This should be contrasted to quenches in the isolated $O(N)$ model, where, to the leading in $1/N$ order, the system does not demonstrate equilibration [46–50].

From the equations of motion, we obtain equilibrium correlators:

$$D_{\mathbf{k}}^{\parallel} = \frac{T}{K\mathbf{k}^2 + 8u\phi^2 + r_{\text{eff}}}, \quad D_{\mathbf{k}}^{\perp} = \frac{T}{K\mathbf{k}^2 + r_{\text{eff}}}. \quad (13)$$

This result is a manifestation of the equipartition theorem. In the symmetry broken phase, where $r_{\text{eff}} = 0$ and $\phi \neq 0$, we observe that the OP equilibrium value ϕ is affected by the thermal fluctuations, cf. Eq. (12). The transverse correlation length $\xi_{\perp} \propto r_{\text{eff}}^{-1/2}$ is indeed divergent. In the disordered phase, $r_{\text{eff}} \neq 0$ and $\phi = 0$, the transverse and longitudinal correlations are not distinguishable.

A useful point of view on the above approximations is as follows. The equations of motion (10)–(11) are equivalent to

$$\frac{d\delta\phi_{\mathbf{k}}^{\perp}(t)}{dt} = -\Gamma(K\mathbf{k}^2 + r_{\text{eff}})\phi_{\mathbf{k}}^{\perp} + \eta_{\mathbf{k}}^{\perp}(t), \quad (14)$$

$$\frac{d\delta\phi_{\mathbf{k}}^{\parallel}(t)}{dt} = -\Gamma(K\mathbf{k}^2 + r_{\text{eff}} + 8u\phi^2)\phi_{\mathbf{k}}^{\parallel} + \eta_{\mathbf{k}}^{\parallel}(t), \quad (15)$$

where $\delta\phi_{\mathbf{k}}^{\alpha}$ represents the fluctuating part of the corresponding Fourier mode $\phi_{\mathbf{k}}^{\alpha}$. We observe that each of the fluctuating modes lives in an effectively parabolic potential, $\langle \delta\phi_{\mathbf{k}}^{\alpha} \rangle = 0$ and the noise term establishes the equilibrium variances given by Eq. (13).

We now formulate the quenching protocol. For simplicity, we assume that the electronic temperature T_e cools down to the equilibrium value T with a constant rate τ_{QP} defined by the electron-phonon coupling. In the usual Landau-Ginzburg theory, the coefficient $r(T_e)$ depends linearly on T_e . To mimic a photoexcitation event, we therefore impose the following dynamics on $r(t)$ – see Fig. 1b:

$$r(t) = r_i + \theta(t) \exp(-t/\tau_{\text{QP}}) \times (r_f - r_i), \quad (16)$$

where $\theta(t)$ is the Heaviside theta function, r_i is the pre-pulse value chosen such that $\phi \neq 0$, and $(r_f - r_i)$ characterizes the strength of the pulse. Below we are interested in the dynamics for time delays much beyond τ_{QP} .

We turn to discuss the internal dynamics that happens to the system as a whole after being quenched, cf. Eq. (16). As mentioned in Fig 1c, we identify four dynamical stages – (i) depletion, (ii) inflation, (iii) mode decoupling and (iv) relaxation to the thermal equilibrium – which we cover below.

In Fig. 3a, we show numerical results for the dynamics of the OP, $\phi(t)$, at different quench strengths. For a weak pump, $\phi(t)$ becomes slightly suppressed and then quickly recovers to the initial value ϕ_0 . This should be contrasted to the case of a strong pulse, for which initially the OP becomes strongly suppressed and then goes through a long

recovery process. The recovery takes longer for stronger pulses – see Fig. 3b. This slowing-down is due to the power-law dynamics $\delta\phi(t) \equiv (\phi(t) - \phi_0) \sim t^{-d_\phi}$, $d_\phi = \frac{3}{2}$.

In Fig. 3c, we plot the evolution of $r_{\text{eff}}(t)$ for different quenches. Note that upon arrival of a laser pulse, $r_{\text{eff}}(+0) = (r_f - r_i)$. This large initial value first decreases due to the time evolution of the “bare value” of $r(t)$, cf. Eq. (16), and later, $t \gtrsim \tau_{\text{QP}}$, due to the dynamics of the OP and collective modes described by Eqs. (9)–(11). Even though $r(t)$ returns to its equilibrium value r_i during a relatively short time τ_{QP} , dynamics of r_{eff} occurs over much longer time scale where it even changes sign, as shown in Fig. 3c. We find that long-time evolution of $r_{\text{eff}} \sim t^{-d_r}$ is power-law-like with $d_r = \frac{5}{2}$. For the fluctuating modes $\delta\phi_{\mathbf{k}}^\alpha$, a large value of r_{eff} implies that each of the effective parabolic potentials becomes initially steeper, and, as such, the noise term in Eqs. (14)–(15) will tend to depopulate these modes – see also Fig. 3d. Therefore, the first stage – depletion – is characterized by suppression of the OP and correlations $D_{\mathbf{k}}^\perp$ and $D_{\mathbf{k}}^\parallel$.

The second stage – inflation – starts when r_{eff} changes

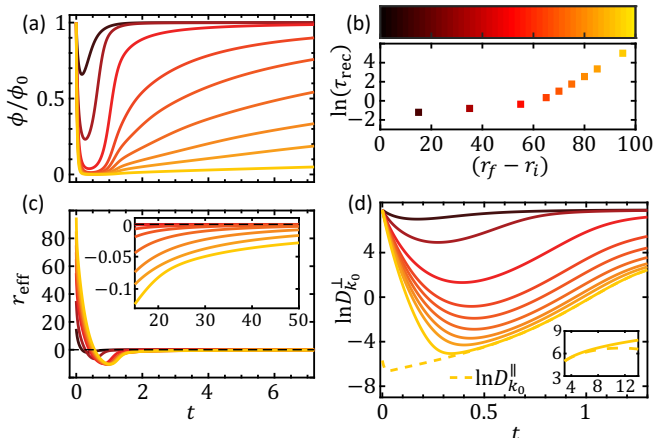


FIG. 3. (Color online) Intrinsic dynamics for different quench strengths, $(r_f - r_i)$. (a) Time dependence of the OP $\phi(t)$ normalized by the pre-pulse value ϕ_0 . At long times, $(\phi(t) - \phi_0) \sim t^{-d_\phi}$ with $d_\phi = \frac{3}{2}$. (b) OP recovery time τ_{rec} . (c) Dynamics of $r_{\text{eff}}(t)$. Initially large positive value of r_{eff} is quickly suppressed and even becomes negative. Then it slowly restores, as a power law $r_{\text{eff}} \sim t^{-d_r}$ with $d_r = \frac{5}{2}$, to the zero value. Inset: Zoomed-in view on the long-time tails. (d) Evolution of $D_{k_0}^\perp$, where $k_0 = \frac{2\pi}{L}$ is the lowest wave vector used in our calculations ($L = 1000$). For a strong pulse, initially $D_{k_0}^\perp$ is suppressed to almost zero, but then, after r_{eff} changes sign, it exponentially proliferates. Dotted line corresponds to $D_{k_0}^\parallel$ for the strongest pulse considered. Note that $D_{k_0}^\parallel$ and $D_{k_0}^\perp$ very soon merge into a single curve indicating that the OP is melted. Inset: longer time dynamics for the strongest pulse. We observe that $D_{k_0}^\parallel$ and $D_{k_0}^\perp$ become distinguishable once the OP value $\phi(t)$ becomes appreciable. Throughout the paper, we use the following parameters: $K = u = 1$, $N = 4$, $\Lambda = \pi$, $\Gamma = 0.5$, $\tau_{\text{QP}} = 0.3$, $r_i = -15$, $T = 0.1$. All panels share the same color scale in (b) for the quench strengths.

its sign. Note that a negative value of r_{eff} implies that each of the effective parabolic potentials becomes more shallow or, as the case for the low-momenta transverse modes, can even become inverted. Therefore, during the inflation, population in each of the modes proliferates, most dramatically for the low-momenta modes – see Fig. 3d. For a given mode $\delta\phi_{\mathbf{k}}^\alpha$, a useful quantity is the time $t_{\mathbf{k}}^\alpha$ when the corresponding occupation $D_{\mathbf{k}}^\alpha$ reaches its maximum: $\frac{d}{dt}D_{\mathbf{k}}^\alpha(t_{\mathbf{k}}^\alpha) = 0$. One can deduce that (i) $t_{\mathbf{k}}^\alpha$ is larger for lower \mathbf{k} , (ii) for a given \mathbf{k} , $t_{\mathbf{k}}^\alpha$ grows with the quench strength, and (iii) $t_{\mathbf{k}}^\perp > t_{\mathbf{k}}^\parallel$.

For a strong quench and at the time when the OP becomes completely suppressed, the longitudinal and transverse correlations are no longer distinguishable – see Fig. 3d. This parallels the disordered phase in equilibrium situation. As the OP develops, these modes start to separate. We will associate the end of the inflation stage with the time $t_{\mathbf{k}=0}^\parallel$, when $D_{\mathbf{k}=0}^\parallel$ reaches its maximum value.

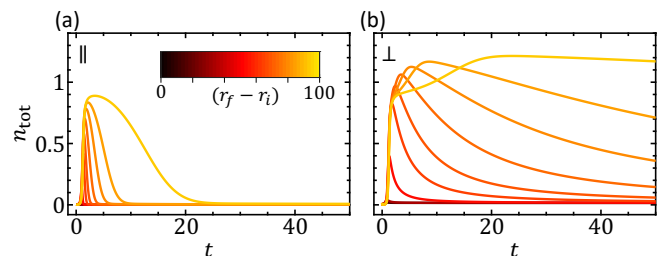


FIG. 4. (Color online) Separation of timescales. (a) Long-time dynamics of the total population of longitudinal modes, $n_{\text{tot}}^\parallel(t)$. (b) The same for transverse modes, $n_{\text{tot}}^\perp(t)$. Note that by the time when n_{tot}^\parallel is nearly fully recovered, n_{tot}^\perp approaches its maximum.

Because of the additional correction to the quadratic term for the longitudinal correlations in Eq. (11), the subsequent evolution – the stage called mode decoupling – is very different for the longitudinal and transverse modes; see Fig. 4. The longitudinal correlations start to relax back to the thermal equilibrium value in Eq. (13), while the transverse modes continue to proliferate, resulting in α , cf. Eq. (3), being positive during the third dynamical stage. Moreover, by the time when n_{tot}^\parallel is sufficiently recovered, n_{tot}^\perp is about to reach its maximum value. Strong experimental evidence of this separation of timescales was reported in Refs. [18, 22, 23].

Just after the mode decoupling, n_{tot}^\perp starts to slowly decrease, cf. Eq. (4), suggesting that the system enters the final relaxation stage. Note that even though lowest-momenta modes $D_{\mathbf{k}}^\perp$ continue to proliferate at very long times, their relative contribution to n_{tot}^\perp is suppressed by the reduced phase space of these modes, which is proportional to k^2 . The underlying dynamics is reminiscent of an inverse particle cascade in the theory of turbulence [8, 51, 52]. The main difference is that in our

system the dynamics is overdamped.

All of the long-time power-law exponents: $\beta = \frac{1}{2}$, $\alpha = -1$, $d_\phi = \frac{3}{2}$, and $d_r = \frac{5}{2}$ – can be deduced merely from the scaling form (2), as we outline in Ref. [45]. However, it is essential to understand why this self-similarity occurs in the first place. Re-establishing the long-range coherence, which is depleted by the laser pulse, is the slowest process that happens in the system, $k_\perp^* \sim t^{-\frac{1}{2}}$. From Fig. 2, we note that the most relevant transverse modes are the ones with wave vectors close to k_\perp^* . For these modes, we can safely neglect fast $r_{\text{eff}} \sim t^{-\frac{5}{2}}$ in Eq. (10) compared to slow $(k_\perp^*)^2 \sim t^{-1}$, resulting in a simple diffusion-like equation with the following solution:

$$\delta D_k^\perp = A_k \exp(-2\Gamma k^2 t), \quad (17)$$

where A_k is yet unknown function of k . As supported by Fig. 3d, $\delta D_k^\perp(t)$ does not diverge for $k \rightarrow 0$. One may then Taylor-expand A_k as $A_k = A_0 + A_2 k^2 + A_4 k^4 + \dots$. The relevant k vectors, the ones in the vicinity of $k_\perp^*(t)$, are small at long times, and, thus, it is safe to leave only the dominant harmonic A_0 in this expansion. For example, one can obtain

$$\begin{aligned} \delta n_{\text{tot}}^\perp \sim (k_\perp^*)^3 \int dx x^2 e^{-x^2} \times \\ \times (A_0 + A_2 x^2 (k_\perp^*)^2 + A_4 x^4 (k_\perp^*)^4 + \dots). \end{aligned} \quad (18)$$

Due to $(k_\perp^*(t))^2 \sim t^{-1}$, indeed contributions from higher harmonics soon become irrelevant. At long times, we can therefore approximate $\delta D_k^\perp \sim \exp(-2\Gamma k^2 t)$, consistent with $\beta = \frac{1}{2}$ and $\alpha = -1$. The above analysis has explained all long-time scalings. Note, however, that the self-similarity in Eq. (2) settles much earlier than the final relaxation stage. It is striking that the functional form of $f(x)$, cf. Eq. (2), is the same for the last two dynamical stages (see Fig. 2), an interesting feature that warrants further investigation.

To test the aforementioned predictions, a variety of experimental setups arranged in a pump-probe scheme could be performed, for example, electron or x-ray diffuse scattering [53–55], resonant inelastic x-ray scattering [14], and Brillouin scattering [56]. These experiments give access to momentum- and/or energy-resolved dynamics of bosonic excitations related to OP, so one may specifically search for signatures of: (i) non-thermal population of the transverse modes, (ii) the self-similarity encoded in Eq. (2), and (iii) different dynamical stages after photoexcitation [see Fig. 1(c)].

For outlook we suggest three possible research directions. First, one can generalize our analysis to systems that have additional conservation laws. For example, in magnetic systems, one may take into account SU(2) symmetry [9] (or approximate symmetry, as is the case for most systems). Second, it is interesting to extend our approach to a fully microscopic model [57–60] in

which one investigates the dynamics of electrons self-consistently rather than phenomenologically. Such microscopics would allow computing other transient properties of the many-body electron systems, for example, various spectral functions that can be probed in time- and angle-resolved photoemission spectroscopy. It would also provide further insights about the interplay between quasiparticles and OP, cf. Eq (16). Finally, one can also take into account coherent dynamics [61, 62], and study, for example, the damping of the Higgs excitations. Exploring the above directions would pave the path towards a more profound understanding of universality in non-equilibrium phase transitions.

The authors would like to thank A. Kogar, B.V. Fine, A.E. Tarkhov, A. Bedrova, V. Kasper, S.L. Johnson, J. Rodriguez-Nieva, J. Marino, A. Schuckert, A. Cavalleri, G. Falkovich, and Z.X. Shen for fruitful discussions. N.G. and A.Z. acknowledge support from the U.S. Department of Energy, BES DMSE and the Skoltech NGP Program (Skoltech-MIT joint project) (analysis and manuscript writing). P.E.D., M.H.M., and E.D. were supported by the Harvard-MIT Center of Ultracold Atoms, AFOSR-MURI Photonic Quantum Matter (award FA95501610323), and DARPA DRINQS program (award D18AC00014).

* Correspondence to: p.dolgirev@g.harvard.edu

- [1] N. Goldenfeld, *Lectures on Phase Transitions and the Renormalization Group* (Addison-Wesley, 1992).
- [2] K. Schwarz, *Phys. Rev. B* **38**, 2398 (1988).
- [3] R. Micha and I. I. Tkachev, *Phys. Rev. Lett.* **90**, 121301 (2003).
- [4] R. Micha and I. I. Tkachev, *Phys. Rev. D* **70**, 043538 (2004).
- [5] J. Berges, A. Rothkopf, and J. Schmidt, *Phys. Rev. Lett.* **101**, 041603 (2008).
- [6] J. Berges and D. Sexty, *Phys. Rev. D* **83**, 085004 (2011).
- [7] B. Nowak, J. Schole, D. Sexty, and T. Gasenzer, *Physical Review A* **85**, 043627 (2012).
- [8] A. P. Orioli, K. Boguslavski, and J. Berges, *Phys. Rev. D* **92**, 025041 (2015).
- [9] S. Bhattacharyya, J. F. Rodriguez-Nieva, and E. Demler, arXiv:1908.00554 (2019).
- [10] S. Erne, R. Bückner, T. Gasenzer, J. Berges, and J. Schmiedmayer, *Nature* **563**, 225 (2018).
- [11] M. Prüfer, P. Kunkel, H. Strobel, S. Lannig, D. Linneemann, C.-M. Schmied, J. Berges, T. Gasenzer, and M. K. Oberthaler, *Nature* **563**, 217 (2018).
- [12] C. Eigen, J. A. Glidden, R. Lopes, E. A. Cornell, R. P. Smith, and Z. Hadzibabic, *Nature* **563**, 221 (2018).
- [13] N. Navon, A. L. Gaunt, R. P. Smith, and Z. Hadzibabic, *Nature* **539**, 72 (2016).
- [14] M. Mitrano, S. Lee, A. A. Husain, L. Delacretaz, M. Zhu, G. de la Peña Muñoz, S. X.-L. Sun, Y. I. Joe, A. H. Reid, S. F. Wandel, *et al.*, *Sci. Adv.* **5**, eaax3346 (2019).
- [15] G. I. Barenblatt and B. G. Isaakovich, *Scaling, self-similarity, and intermediate asymptotics: dimensional*

- analysis and intermediate asymptotics*, Vol. 14 (Cambridge University Press, 1996).
- [16] A. Tomeljak, H. Schaefer, D. Stadtter, M. Beyer, K. Biljakovic, and J. Demsar, *Phys. Rev. Lett.* **102**, 066404 (2009).
- [17] F. Schmitt, P. S. Kirchmann, U. Bovensiepen, R. Moore, J. Chu, D. Lu, L. Rettig, M. Wolf, I. Fisher, and Z. Shen, *New J. Phys.* **13**, 063022 (2011).
- [18] A. Zong, A. Kogar, Y.-Q. Bie, T. Rohwer, C. Lee, E. Baldini, E. Ergeen, M. B. Yilmaz, B. Freelon, E. J. Sie, *et al.*, *Nat. Phys.* **15**, 27 (2019).
- [19] A. Kogar, A. Zong, P. E. Dolgirev, X. Shen, J. Straquadine, Y.-Q. Bie, X. Wang, T. Rohwer, I. Tung, Y. Yang, *et al.*, arXiv eprint:1904.07472 (2019).
- [20] F. Zhou, J. Williams, C. D. Malliakas, M. G. Kanatzidis, A. F. Kemper, and C.-Y. Ruan, arXiv eprint:1904.07120 (2019).
- [21] E. Mohr-Vorobeva, S. L. Johnson, P. Beaud, U. Staub, R. De Souza, C. Milne, G. Ingold, J. Demsar, H. Schaefer, and A. Titov, *Phys. Rev. Lett.* **107**, 036403 (2011).
- [22] C. Laulhe, T. Huber, G. Lantz, A. Ferrer, S. O. Mariager, S. Grubel, J. Rittmann, J. A. Johnson, V. Esposito, A. Lubcke, *et al.*, *Phys. Rev. Lett.* **118**, 247401 (2017).
- [23] S. Vogelgesang, G. Storeck, J. Horstmann, T. Diekmann, M. Sivis, S. Schramm, K. Rossnagel, S. Schafer, and C. Ropers, *Nat. Phys.* **14**, 184 (2018).
- [24] T. Huber, S. O. Mariager, A. Ferrer, H. Schafer, J. A. Johnson, S. Grubel, A. Lubcke, L. Huber, T. Kubacka, C. Dornes, *et al.*, *Phys. Rev. Lett.* **113**, 026401 (2014).
- [25] G. Storeck, J. G. Horstmann, T. Diekmann, S. Vogelgesang, G. von Witte, S. Yalunin, K. Rossnagel, and C. Ropers, arXiv:1909.10793 (2019).
- [26] S. Hellmann, T. Rohwer, M. Kallane, K. Hanff, C. Sohrt, A. Stange, A. Carr, M. Murnane, H. Kapteyn, L. Kipp, *et al.*, *Nat. Commun.* **3**, 1069 (2012).
- [27] K. Okazaki, Y. Ogawa, T. Suzuki, T. Yamamoto, T. Someya, S. Michimae, M. Watanabe, Y. Lu, M. Nohara, H. Takagi, *et al.*, *Nat. Commun.* **9**, 4322 (2018).
- [28] A. Kirilyuk, A. V. Kimel, and T. Rasing, *Rev. Mod. Phys.* **82**, 2731 (2010).
- [29] M. Dean, Y. Cao, X. Liu, S. Wall, D. Zhu, R. Mankowsky, V. Thampy, X. Chen, J. Vale, D. Casa, *et al.*, *Nat. Mater.* **15**, 601 (2016).
- [30] S. Mariager, C. Dornes, J. Johnson, A. Ferrer, S. Grubel, T. Huber, A. Caviezel, S. Johnson, T. Eichhorn, G. Jakob, *et al.*, *Phys. Rev. B* **90**, 161103 (2014).
- [31] P. Beaud, A. Caviezel, S. O. Mariager, L. Rettig, G. Ingold, C. Dornes, S.-W. Huang, J. A. Johnson, M. Radovic, T. Huber, *et al.*, *Nat. Mater.* **13**, 923 (2014).
- [32] Z. Tao, T.-R. T. Han, and C.-Y. Ruan, *Phys. Rev. B* **87**, 235124 (2013).
- [33] B. Mansart, D. Boschetto, A. Savoia, F. Rullier-Albenque, F. Bouquet, E. Papalazarou, A. Forget, D. Colson, A. Rousse, and M. Marsi, *Phys. Rev. B* **82**, 024513 (2010).
- [34] L. Perfetti, P. Loukakos, M. Lisowski, U. Bovensiepen, H. Eisaki, and M. Wolf, *Phys. Rev. Lett.* **99**, 197001 (2007).
- [35] P. E. Dolgirev, A. Rozhkov, A. Zong, A. Kogar, N. Gedik, and B. V. Fine, arXiv eprint:1904.09795 (2019).
- [36] S. L. Johnson, M. Savoini, P. Beaud, G. Ingold, U. Staub, F. Carbone, L. Castiglioni, M. Hengsberger, and J. Osterwalder, *Struct. Dyn.* **4**, 061506 (2017).
- [37] Since OP degrees of freedom are composed of electrons and phonons, the introduction of three subsystems might be confusing. For this reason, in CDW systems one sometimes splits the lattice into two groups: (i) phonons associated with the OP and (ii) the rest of the lattice. One then describes a non-equilibrium state by assigning different temperatures to each subsystem.
- [38] N. Gedik, P. Blake, R. Spitzer, J. Orenstein, R. Liang, D. Bonn, and W. Hardy, *Phys. Rev. B* **70**, 014504 (2004).
- [39] P. Kusar, V. V. Kabanov, J. Demsar, T. Mertelj, S. Sugai, and D. Mihailovic, *Phys. Rev. Lett.* **101**, 227001 (2008).
- [40] R. P. Prasankumar and A. J. Taylor, *Optical techniques for solid-state materials characterization* (CRC Press, 2016).
- [41] F. Boschini, E. da Silva Neto, E. Razzoli, M. Zonno, S. Peli, R. Day, M. Michiardi, M. Schneider, B. Zwartsenberg, P. Nigge, *et al.*, *Nat. Mater.* **17**, 416 (2018).
- [42] A. J. Bray, *Adv. Phys.* **51**, 481 (2002).
- [43] P. C. Hohenberg and B. I. Halperin, *Rev. Mod. Phys.* **49**, 435 (1977).
- [44] Z. Sun and A. J. Millis, arXiv eprint: 1905.05341 (2019).
- [45] See supplemental materials for more details.
- [46] A. Chandran, A. Nanduri, S. S. Gubser, and S. L. Sondhi, *Phys. Rev. B* **88**, 024306 (2013).
- [47] B. Sciolla and G. Biroli, *Phys. Rev. B* **88**, 201110 (2013).
- [48] A. Chiochetta, M. Tavora, A. Gambassi, and A. Mitra, *Phys. Rev. B* **91**, 220302 (2015).
- [49] A. Maraga, A. Chiochetta, A. Mitra, and A. Gambassi, *Phys. Rev. E* **92**, 042151 (2015).
- [50] A. Chiochetta, M. Tavora, A. Gambassi, and A. Mitra, *Phys. Rev. B* **94**, 134311 (2016).
- [51] V. E. Zakharov, V. S. L’vov, and G. Falkovich, *Kolmogorov spectra of turbulence I: Wave turbulence* (Springer Science & Business Media, 2012).
- [52] S. Nazarenko, *Wave turbulence*, Vol. 825 (Springer Science & Business Media, 2011).
- [53] T. Chase, M. Trigo, A. H. Reid, R. Li, T. Vecchione, X. Shen, S. Weathersby, R. Coffee, N. Hartmann, D. A. Reis, X. J. Wang, and H. A. Durr, *Appl. Phys. Lett.* **108**, 041909 (2016).
- [54] S. Wall, S. Yang, L. Vidas, M. Chollet, J. M. Glownia, M. Kozina, T. Katayama, T. Henighan, M. Jiang, T. A. Miller, *et al.*, *Science* **362**, 572 (2018).
- [55] M. J. Stern, L. P. Rene de Cotret, M. R. Otto, R. P. Chatelain, J.-P. Boisvert, M. Sutton, and B. J. Siwick, *Phys. Rev. B* **97**, 165416 (2018).
- [56] S. O. Demokritov, B. Hillebrands, and A. N. Slavin, *Phys. Rep.* **348**, 441 (2001).
- [57] M. Babadi, E. Demler, and M. Knap, *Phys. Rev. X* **5**, 041005 (2015).
- [58] M. Babadi, M. Knap, I. Martin, G. Refael, and E. Demler, *Phys. Rev. B* **96**, 014512 (2017).
- [59] Y. Lemonik and A. Mitra, *Phys. Rev. Lett.* **121**, 067001 (2018).
- [60] Y. Lemonik and A. Mitra, *Phys. Rev. B* **100**, 094503 (2019).
- [61] P. Gagel, P. P. Orth, and J. Schmalian, *Phys. Rev. Lett.* **113**, 220401 (2014).
- [62] P. Gagel, P. P. Orth, and J. Schmalian, *Phys. Rev. B* **92**, 115121 (2015).

SUPPLEMENTAL MATERIALS

I. Derivation of the equations of motion

Here we provide details of the derivation of the main Eqs. (9)–(12).

Dynamics of ϕ . Evolution of the field $\phi = \frac{1}{\sqrt{V}}\phi_{1,\mathbf{q}=0}$ can be obtained from:

$$\partial_t \langle \phi_{\alpha,\mathbf{q}} \rangle_t = \int D[\phi] \phi_{\alpha,\mathbf{q}} \partial_t \mathcal{P}([\phi], t) = -\Gamma \left\langle \frac{\delta \mathcal{F}}{\delta \phi_{\alpha,-\mathbf{q}}} \right\rangle, \quad (\text{S1})$$

where in the last equality we used the Fokker-Planck Eq. (8), and integration by parts. The latter derivative can be calculated from Eq. (6):

$$\frac{\delta \mathcal{F}}{\delta \phi_{\alpha,-\mathbf{q}}} = (r + K\mathbf{q}^2) \phi_{\alpha,\mathbf{q}} + \frac{4u}{V} \sum_{\mathbf{k}_1, \mathbf{k}_2} \phi_{\beta,\mathbf{k}_1} \phi_{\beta,\mathbf{k}_2} \phi_{\alpha,\mathbf{q}-\mathbf{k}_1-\mathbf{k}_2}. \quad (\text{S2})$$

Using Wick's theorem and leaving only terms up to the leading order in $1/N$, we obtain

$$\left\langle \sum_{\mathbf{k}_1, \mathbf{k}_2} \phi_{\beta,\mathbf{k}_1} \phi_{\beta,\mathbf{k}_2} \phi_{1,-\mathbf{k}_1-\mathbf{k}_2} \right\rangle \approx \phi_{1,\mathbf{q}=0}^3 + \phi_{1,\mathbf{q}=0} \sum_{\mathbf{k}} (D_{\mathbf{k}}^{\parallel} + (N-1)D_{\mathbf{k}}^{\perp}). \quad (\text{S3})$$

Combining Eq. (S1) and Eq. (S3) we arrive at Eq. (9) of the main text.

Dynamics of the correlators. Applying the same trick as above, we derive:

$$\begin{aligned} \partial_t \langle \phi_{\alpha,\mathbf{k}} \phi_{\alpha,-\mathbf{k}} \rangle_c &= 2T\Gamma - 2\Gamma \times \\ &\times \left[\left\langle \phi_{\alpha,\mathbf{k}} \frac{\delta \mathcal{F}}{\delta \phi_{\alpha,\mathbf{k}}} \right\rangle - \langle \phi_{\alpha,\mathbf{k}} \rangle \left\langle \frac{\delta \mathcal{F}}{\delta \phi_{\alpha,\mathbf{k}}} \right\rangle \right]. \end{aligned} \quad (\text{S4})$$

For the case of the transverse component, in the leading in $1/N$ order we obtain:

$$\begin{aligned} \left\langle \phi_{\alpha,\mathbf{k}} \sum_{\mathbf{k}_1, \mathbf{k}_2} \phi_{\beta,\mathbf{k}_1} \phi_{\beta,\mathbf{k}_2} \phi_{\alpha,-\mathbf{k}-\mathbf{k}_1-\mathbf{k}_2} \right\rangle &\approx \\ \approx D_{\mathbf{k}}^{\perp} \left(\phi_{1,\mathbf{q}=0}^2 + \sum_{\mathbf{q}} (D_{\mathbf{q}}^{\parallel} + (N-1)D_{\mathbf{q}}^{\perp}) \right). \end{aligned} \quad (\text{S5})$$

Combining Eq. (S4) and Eq. (S5) we arrive at Eq. (10) of the main text. For the case of the longitudinal component, similarly to the above discussion we get

$$\begin{aligned} \sum_{\mathbf{k}_1, \mathbf{k}_2} \left(\langle \phi_{1,\mathbf{k}} \phi_{\beta,\mathbf{k}_1} \phi_{\beta,\mathbf{k}_2} \phi_{1,-\mathbf{k}-\mathbf{k}_1-\mathbf{k}_2} \rangle - \langle \phi_{1,\mathbf{k}} \rangle \langle \phi_{\beta,\mathbf{k}_1} \phi_{\beta,\mathbf{k}_2} \phi_{1,-\mathbf{k}-\mathbf{k}_1-\mathbf{k}_2} \rangle \right) &\approx \\ \approx D_{\mathbf{k}}^{\parallel} \left(3\phi_{1,\mathbf{q}=0}^2 + \sum_{\mathbf{q}} (D_{\mathbf{q}}^{\parallel} + (N-1)D_{\mathbf{q}}^{\perp}) \right). \end{aligned} \quad (\text{S6})$$

This equation leads to Eq. (11).

II. LONG-TIME SELF-SIMILARITY

Transverse correlations

In the main text, we presented the derivation of the long-time exponents $\beta = \frac{1}{2}$ and $\alpha = -1$. Here we derive $d_r = \frac{5}{2}$ and $d_\phi = \frac{3}{2}$ starting from the scaling form (2) and using the equations of motion.

To extract the value of d_r , we need to consider the interplay between the order parameter and the transverse correlations (longitudinal correlations can be ignored, cf. Fig. 4). Assuming that at long times $r_{\text{eff}} \sim t^{-d_r}$, the equation of motion (9) reads

$$\frac{d\delta\phi}{dt} = -\Gamma r_{\text{eff}}(t)\phi \sim t^{-d_r}, \quad (\text{S7})$$

where we implied that the order parameter $\phi(t) = \phi_{\text{eq}} + \delta\phi(t)$ is already close to its equilibrium value ϕ_{eq} . Integrating the above equation, we obtain $\phi^2(t) \approx \phi_{\text{eq}}^2 + Ct^{-d_\phi}$, where C is some constant and $d_\phi = d_r - 1$. Note that since $\phi^2(t)$ enters the definition of $r_{\text{eff}}(t)$, cf. Eq. (12), the more dominant scaling t^{-d_r+1} from the order parameter must be compensated by the transverse correlations. From the scaling (2) we note that

$$\delta n_{\text{tot}}^{\perp} \sim t^\alpha \int dk f(kt^\beta) \sim t^{\alpha-\beta}. \quad (\text{S8})$$

Therefore, we have

$$\alpha - \beta = -d_r + 1 \Rightarrow d_r = 1 + \beta - \alpha = \frac{5}{2}. \quad (\text{S9})$$

This result also gives $d_\phi = d_r - 1 = \frac{3}{2}$. It is encouraging to see that all of the universal (independent from the microscopic parameters such as Γ , τ_{QP} , T , u and K) scaling exponents can be obtained from a single assumption in Eq. (2).

Longitudinal correlations

During the evolution, the longitudinal correlation function $D_{\mathbf{k}}^{\parallel}$ remains bell-shaped with a maximum at $k = 0$ suggesting to define $\tilde{g}(t) = D_{k=0}^{\parallel}(t)$ and $k_{\parallel}^*(t)$ to be the wave vector corresponding to half width at half maximum in $D_{\mathbf{k}}^{\parallel}$. Notably, both functions at long times behave as $\tilde{g}(t)$, $k_{\parallel}^*(t) \sim t^{-d_\phi}$ – see Fig. S1. We also observe that this power-law exponent implies that the longitudinal correlations exhibit the leading scaling (see the previous subsection), i.e. these modes should not be entirely ignored.

To explain the above observation, we note that at long times, when the order parameter $\phi(t) = \phi_0 + \delta\phi$ is already close to be recovered, the equation of motion (11) can be approximated to (we fix $K = 1$ for convenience)

$$\frac{d\delta D_{\mathbf{k}}^{\parallel}}{dt} \approx -32\Gamma u \phi_0 \delta\phi D_{\mathbf{k},\text{eq}}^{\parallel} - 2\Gamma(k^2 + 8u\phi_0^2)\delta D_{\mathbf{k}}^{\parallel}, \quad (\text{S10})$$

where $D_{\mathbf{k}}^{\parallel}(t) = D_{\mathbf{k},\text{eq}}^{\parallel} + \delta D_{\mathbf{k}}^{\parallel}(t)$ and we disregarded fast $r_{\text{eff}}(t) \sim t^{-d_r}$ compared to slow $\delta\phi(t) \sim t^{-d_\phi}$ ($0 < d_\phi < d_r$, see previous subsection). The above equation can be solved analytically. Indeed, substituting

$$\delta D_{\mathbf{k}}^{\parallel}(t) = e^{-2\Gamma(k^2+8u\phi_0^2)t} h_{\mathbf{k}}(t) \quad (\text{S11})$$

we obtain the following equation on $h_{\mathbf{k}}(t)$:

$$\frac{dh_{\mathbf{k}}}{dt} = -32\Gamma u\phi_0\delta\phi D_{\mathbf{k},\text{eq}}^{\parallel} e^{2\Gamma(k^2+8u\phi_0^2)t}. \quad (\text{S12})$$

Integration of this equation gives

$$h_{\mathbf{k}}(t) = h_{\mathbf{k}}(t_0) + \frac{C}{k^2 + 8u\phi_0^2} \int_{t_0}^t dt' \frac{e^{2\Gamma(k^2+8u\phi_0^2)t'}}{(t')^{d_\phi}}, \quad (\text{S13})$$

where C is some constant. We, therefore, conclude that

$$\delta D_{\mathbf{k}}^{\parallel} = \delta D_{\mathbf{k}}^{\parallel,(1)} + \delta D_{\mathbf{k}}^{\parallel,(2)}, \quad (\text{S14})$$

where $\delta D_{\mathbf{k}}^{\parallel,(1)}(t) = h_{\mathbf{k}}(t_0)e^{-2\Gamma(k^2+8u\phi_0^2)t}$ decays exponentially in time, whereas

$$\delta D_{\mathbf{k}}^{\parallel,(2)} \sim \frac{e^{-2\Gamma(k^2+8u\phi_0^2)t}}{k^2 + 8u\phi_0^2} \int_{t_0}^t dt' \frac{e^{2\Gamma(k^2+8u\phi_0^2)t'}}{(t')^{d_\phi}} \quad (\text{S15})$$

is potentially important.

At long times $t \rightarrow \infty$, we observe that

$$F(t) \equiv \int_{t_0}^t dt' \frac{e^{at'}}{(t')^b} \sim \frac{e^{at}}{t^b}, \quad a, b > 0. \quad (\text{S16})$$

Indeed, by differentiating $F(t)$ we note that it satisfies

$$\frac{dF}{dt} = \frac{e^{at}}{t^b}. \quad (\text{S17})$$

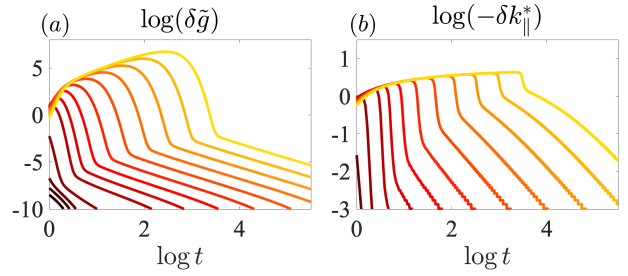


FIG. S1. (a) evolution of the scaling function $\delta\tilde{g}(t) \equiv \tilde{g}(t) - \tilde{g}_{\text{eq}}$ for different quenches. (b) the same for the longitudinal wave vector $\delta k_{\parallel}^*(t) \equiv k_{\parallel}^*(t) - k_{\parallel,\text{eq}}^*$. The second (inflation) and the third (mode decoupling) stages of the overall dynamics are clearly seen. At long times, both functions scale as $\delta\tilde{g}(t), \delta k_{\parallel}^*(t) \sim t^{-d_\phi}$.

By substituting $F(t) = e^{at}p(t)$ we separate rapid exponential growth from slow power-law-like dynamics encoded in $p(t)$:

$$\frac{dp}{dt} + ap = \frac{1}{t^b}. \quad (\text{S18})$$

From this equation, we finally see that $p \sim t^{-b}$ (as long as $a \neq 0$). Combining Eqs. (S15) and (S16), we conclude that

$$\delta D_{\mathbf{k}}^{\parallel,(2)} \sim \frac{t^{-d_\phi}}{k^2 + 8u\phi_0^2}, \quad (\text{S19})$$

i.e. indeed $\delta D_{\mathbf{k}}^{\parallel}$ gets power-law-like contribution with the leading exponent. For completeness, we also note that

$$\delta n_{\text{tot}}^{\parallel,(2)} = \int \frac{d^3\mathbf{k}}{(2\pi)^3} \delta D_{\mathbf{k}}^{\parallel,(2)} \sim t^{-d_\phi} \quad (\text{S20})$$

also exhibits the same scaling.